Empirical anisotropic spectral reflectance model for snow derived from DAIS-7915 airborne spectrometer data

Rune Solberg

Norwegian Computing Center

P.O. Box 114 Blindern, N-0314 Oslo, Norway

Phone: +47 2285 2500; Fax: +47 2269 7660; E-mail: rune.solberg@nr.no

Abstract: Modeling the anisotropic reflectance of snow will be important for various applications, like climatology, meteorology and water management. Accurate climatic and meteorological modeling of energy balance needs to take the anisotropic effect into account. This is also the case for accurate snow-cover mapping for water management. This paper describes the development of an empirical model for the anisotropic spectral reflectance of snow based on airborne DAIS-7915 spectrometer data covering the spectral range 0.4-12.6 micrometer. The data set used is from the Jotunheimen mountain area in Norway. Flight lines were in the solar plane and orthogonal to this, and a swath angle range of ±26 degrees was obtained. Combined with the effect of terrain slopes, an actual terrain incidence angle range of ±40 degrees was obtained. An accurate terrain model was derived from digital aerial photographs. Areas without snow were masked out based on another infrared high-resolution digital aerial orthophoto. Field measurements confirmed homogeneous conditions allowing a large area of data to be used. Field measurements were also applied for calibration. The raw angle-to-reflectance data were smoothed and represented in a 3D data storage model for further applications. The observation angles varied between –45° and 36° and the solar zenith angle varied between 24° and 55°. A hot-spot region representing forward scattering showed about 8% increase in radiance values. This anisotropy remained constant up to wavelengths of about 1700 nm. No anisotropic effects were detectable beyond this wavelength.

INTRODUCTION

Snow reflects sunlight in an anisotropic manner with a strength depending on the snow's metamorphosis stage. New snow and powder snow show least anisotropic effects, while they increase with the grain size (older snow). The result is strong forward scattering and often a small peak backward in the solar plane [1], [2]. Grain shape also plays an important role.

The anisotropic behavior of snow has been studied in several works at various scales based on field, airborne and spaceborne measurements. Various field experiments have studied and quantified the effect for different snow types at visual and near-infrared wavelengths (350-1100 nm), see, e.g., [1]-[4]. Anisotropic effects were studied in [5] using an airborne spectroradiometer covering the range 462-866 nm, also including different types of vegetation extending above the snow surface. The study in [4] also includes the mid-infrared wavelengths covered by Landsat TM bands 5 and 7.

A quantification of the anisotropic effects throughout the optical spectrum for various snow types is needed for various applications. Both albedo and snow-cover mapping is affected. Accurate albedo measurements are important for accurate weather and climate modeling. The incoming energy (solar irradiance) will be unevenly distributed while being reflected from the surface (surface radiance) with a magnitude depending on the solar zenith angle and the snow state.

While doing snow-cover mapping, the snow surface is usually assumed to have the same spectral reflectance for the whole scene. However, in practice it may vary quite a lot depending on the solar zenith angle and sensor-viewing angle. Extreme effects have been observed for regular snow-cover mapping of the Norwegian mountains for water management applications while using early morning scenes from NOAA AVHRR. The AVHRR has a maximum scan angle of 55°, which combined with large solar zenith angles results in a snow illumination-observation geometry giving much higher reflection. The result is virtually much higher snow coverage for parts of early morning scenes than the same parts of mid-day scenes when using an algorithm with one single calibration value.

The local topography makes the situation even more complicated. The local illumination-observation geometry will vary with a terrain point's slope and aspect. If the topography is not taken into account, energy distribution modeling and snow-cover retrieval will be more or less affected by errors depending on the amount of terrain relief.

A complete mapping of the snow's anisotropic reflection in the optical spectrum for all geometries of illumination and observation, and also covering all common snow types, is an extremely comprehensive task and remains to be accomplished. When it is finally established, more accurate weather and climate modeling and snow-cover mapping will be possible. This work contributes to that task by covering a large spectral range.

The work has been done within SNOWTOOLS, a project within the European Union's Environment and Climate research program. Multi-purpose data sets for optical and microwave snow parameter retrieval were acquired in the period 1997-99 and accompanied by field campaigns. A summary of the project results may be found in [6].

The study area was covered by a 79 band airborne spectrometer DAIS 7915 (Digital Airborne Imaging Spectrometer). Together with the airborne synthetic aperture radar EMISAR, these sensors comprise the European Airborne Sensing Capabilities (EARSeC) developed as an initiative by the European Union. The spectrometer was built by Geophysical Research corp.

(GER), USA, and has been improved by Deutsches Zentrum für Luft und Raumfart e.V. (DLR), Germany. Due to requirements for very accurate calibration, a calibration laboratory was built at DLR. Two flight periods were accomplished in 1997 and 1998 as part of a European-wide campaign.

METHODOLOGY

The approached applied here has been to reconstruct the local illumination and observation geometry for each pixel. This includes taking into account the terrain surface geometry. For all pixels with the same geometrical conditions, the mean directional reflectance is calculated. The result is organized into a bidirectional reflectance distribution function (BRDF) data cube with the dimensions *observation zenith angle*, *solar zenith angle*, and *wavelength*. There is one such data cube for each azimuth plane. The procedure applied is explained in more detail in the following.

Two parameters had to be calculated for each pixel: The local solar zenith angle, α_s, and the local observation angle, α_o. The parameters are calculated in the relevant azimuth planes, P, either the solar plane, P_s (also called the principal plane) or the solar-perpendicular plane, P_a. Both parameters need an accurate digital terrain model (DTM) to be calculated.

A digital elevation model (DEM) was applied to determine the terrain surface normal. First, the slope and aspect for each individual pixel were determined by fitting a plane to a centered square of 3×3 pixels. The normal vector to the plane is then an estimate of the terrain normal, *t*.

The calculation of the local solar pointing unit vector, *s*, is based on a polynomial approximation for determining the Sun's geocentric position. The geocentric solar coordinates, right ascension and declination, are determined from the exact Julian date of the image acquisition time. The Earth's shape is approximated by an ellipsoid, and the Sun's elevation and azimuth is calculated for the given geographical location. This gives the vector *s* directly.

All calculations that follow have been done within the selected azimuth plane, P. The local solar zenith angle, α_s, is the angular difference between *s* and *n* in the plane P.

The local observation angle is calculated in several steps:

1. A sensor-scanning-pattern model is used to calculate the geodetic observation angle, α_{go}, for all pixels in the image. This is the observation angle for flat terrain.
2. The scanning plane's local terrain slope, α_t. is calculated by projecting the vector *n* into this plane.
3. The observation angle is then given by the combined angle $\alpha_o = \alpha_{go} + \alpha_t$.

Due to partial snow coverage, a snow mask, M_s, with the classes *snow* and *snow free* surface had to be generated. In order to avoid mixed pixels along the borders, the morphological operator *erode* was applied once onto the mask removing the original border pixels.

The remaining task is to map all radiance values from the image space into the BRDF-radiance-cube space. This is done by the following assignment:

$$I_{DAIS}(x, y, \lambda) \rightarrow R_{BRDF}(\alpha_o, \alpha_s, \lambda) \mid M_s(x, y) > 0 \qquad (1)$$

where $\rightarrow$ here means incremental update of the mean radiance value in R_{BRDF} by the new value I_{DAIS} with pixel coordinates (x, y) if the pixel represents snow as given by M_s. A population image, I_P, has been used to store the current number of pixels applied in R_{BRDF} for each location $(\alpha_o, \alpha_s, \lambda)$.

THE DATA SET

The study area, Heimdalen, is located in the Jotunheimen mountain area in Norway (9.0° E; 61.4° N). The area is of about 100 km² with an elevation range of 1050-1840 m a.s.l. The area is free of tall vegetation except for some birch in the lowest locations (not within applied data).

Heimdalen was covered by DAIS 7915 image acquisition on 21 June 1998 between about 8:13 and 9:31 GMT (about 9:30-10:50 true solar time). The imaging spectrometer has 79 bands covering the spectral range 0.4-12.6 µm. Some sensor characteristics are given in Table 1. The dynamic range is 15 bits. The sensor scans with a swath angle of ±26° generating lines of 512 pixels. The flight altitude was fixed such that the mean pixel size was 5×5 m². Ten stripes, of a total length of 90 km of data with a swath with of 2.5 km, were acquired. Seven stripes were oriented with flight direction parallel to the solar plane, thereby minimizing the anisotropic reflectance, while three stripes were flown perpendicular to the solar plane in order to maximize the anisotropic reflectance. The three latter stripes were dedicated to this study, while the other had multiple purposes. The number of pixel samples in these three stripes is totaling 2.3 million.

A digital elevation model (DEM) was generated for the whole area based on 1:40,000 scale aerial photos acquired under snow-free conditions 15 August 1998. The 14 photographs from two stripes were scanned, and a block of stereo models generated using a digital photogrammetric workstation. Automatic co-registration of image pairs was done, followed by manual absolute orientation using ground control points. Terrain elevation was then derived for 5×5 m² pixels with a height accuracy of about 1 m.

In order to get an accurate map of the snow cover, aerial photographs were acquired simultaneously with the DAIS data. A similar flight plan and data processing procedure as for the DEM generation was followed. The result was a 1 m spatial resolution orthophoto covering the whole study area.

Table 1. Spectral characteristics of DAIS 7915

Wavelength interval (µm)	Number of bands	Bandwidth
0.4-1.0	32	15-30 nm
1.5-1.8	8	45 nm
2.0-2.5	32	20 nm
3.0-5.0	1	2.0 µm
8.0-12.6	6	0.9 µm

A snow mask was derived from DAIS band 25 (center wavelength 912 nm) and controlled against the orthophoto. The orthophoto could also have been used, but this approach was avoided in order to minimize the number of data sets to co-register.

A field campaign was carried out during the image acquisition. Two field teams measured the snow parameters grain size, wetness, density, temperature and the spectral reflectance by a FieldSpec spectroradiometer covering the spectral range 350-2500 nm. In addition the air temperature was measured. The snow parameters were measured at nine different point locations. Complementary ground temperature measurements were done at seven snow-free locations using a digital thermometer with physical ground contact and an IR thermometer with spectral coverage 7-16 μm. The location of each point was determined by GPS.

RESULTS

The field conditions were very favorable for such a study with homogeneous snow characteristics. The snow was fairly wet in the whole area with snow that had undergone a longer period of metamorphosis. The variations in snow density were typically 5-10%, and the grain sizes were in the range 1.5-2 mm at all locations. This means that combining radiance measurements with the same illumination and observation geometry for different geographical locations should not introduce significant errors due to heterogeneous snow.

The weather was also excellent with about 99% cloud-free conditions for nine of the image stripes. The stripes used for this study had no clouds.

One advantage of the R_{BRDF} cube is that various sub-spaces, i.e., different combinations of dimensions or variables, can easily be combined and extracted for visualization. Of particular interest is:

$$R_{BRDF}(\alpha_o, \alpha_s) \mid \lambda \text{ constant} \qquad (2)$$

$$R_{BRDF}(\alpha_o, \lambda) \mid \alpha_s \text{ constant} \qquad (3)$$

An example of (2) is shown in Figure 1 for λ = 1034 nm (band 32). Most of the data is within a bounding box of $-45° < \alpha_o < 36°$ and $24° < \alpha_s < 55°$. There are a lot of local variations in the radiance in the area, however, there are some clear large-scale variations. A hot-spot region is clearly visible in the upper left of the data area. The hot-spot region follows the diagonal line of equal (α_o, α_s) values (forward scattering corresponding to mirror reflection). The radiance values in the hot-spot region are typically 8% higher than for similar areas outside the region. Unfortunately, the diagonal of equal $(-\alpha_o, \alpha_s)$ values is not covered by the data set, so there is no information about any backward scattering. Furthermore, there is a clear trend of increasing radiance along the α_s axis in direction of α_s = 0° (zenith) due to the Lambertian component of the reflection. The radiance increases by 27% from α_s = 51° to α_s = 26°.
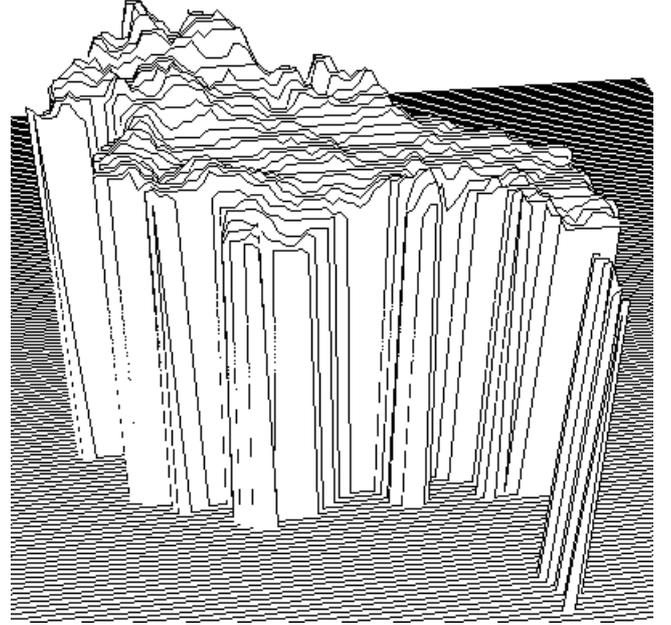

Figure 1. Radiance values for a (α_o, α_s) sub-space at λ = 1034 nm. The direction of α_o is left/right, while α_s in the direction zenith goes into the the figure.

An inspection of (α_o, λ) sub-spaces shows saturated radiance values for bands 1-13 (501-705 nm). The contrast between the hot spot and other areas of about the same α_s keeps constant for bands 14-40 (722-1729 nm). However, the contrast along the α_s axis increases by about 20% within this spectral region for α_s = 51°-26°. Beyond band 41 (2004 nm) both the Lambertian effect and anisotropy disappears completely in the data. For bands 41-72 (2004-2490 nm), there are a lot of extreme variations in data values (over the whole dynamic range) in an apparently random pattern. It has not been possible to explain these variations. Bands 74-79 (8747-12668 nm) shows very little variations at all, which confirms the homogeneous situation of melting snow in the whole area.

DISCUSSION AND CONCLUSIONS

Hyperspectral snow data has been acquired over a Norwegian mountain area using an airborne imaging spectrometer, DAIS 7915, covering the spectral range 0,4-12,6 μm. The data was radiometrically calibrated to radiance. The snow was well-developed (old), wet and with very homogeneous characteristics in the area. For each pixel, the illumination-observation geometry was reconstructed. The image data was transferred to a radiance cube with the dimensions observation zenith angle, solar zenith angle and wavelength. There is one such cube for each azimuth plane (principal plane, perpendicular plane). Pixels with the same geometry were averaged. The data set may be used for investigation of anisotropic effects in itself, and applied as an empirical model to predict correct reflectance values for snow-cover mapping and albedo retrieval related to water management and meteorological and climatological applications.

A complete mapping of the snow's anisotropic effects is an extremely comprehensive task, and every data set published so far is very restricted. This data set has its main limitations in the illumination-observation geometry and snow characteristics. The topography is used to extend the angular ranges of the geometry. However, the forward and backward scattering is highest for very low solar elevations, which was not practical possible to cover here. The only snow situation covered was wet, heavily metamorphosed snow. However, this type of snow has shown to be most problematic for snow-cover mapping. The main advantage of the data set is the wide spectral range covered.

The main error source is probably related to the co-registration of the DEM and the DAIS images. This was done by the use of ground control points and a 2nd degree polynomial geometrical transformation. There are plans to apply a simulator to model the flight geometry better and then rerun the image acquisition model in order to generate a new radiance cube to ensure the highest possible quality of the data set. However, the trends in the data set as it is now should not be affected, only the exact quantification.

It may also be seen as a deficit that no atmospheric correction has been done in order to convert the data to at-surface reflectance. However, there are also always uncertainties with atmospheric correction if the exact atmospheric characteristics are not known along the radiation paths. Conversion may be done later if applications require it.

The work presented here is currently followed up by a field-based hyperspectral measurement project aiming to cover all relevant illumination-observation geometries for the most common snow types. That study is covering the 350-2500 nm spectral range.

The DAIS BRDF cube will be made available at the SNOWTOOLS Internet-based spectral snow database located at http://terr2.unibe.ch/snowtools/.

ACNOWLEDGMENTS

REFERENCES

[1] J. Dozier, R.E. Davis, A.T.C. Chang and K. Brown, "The spectral bidirectional reflectance of snow," Proceedings of the 4th International Colloquium on Spectral Signatures of Objects in Remote Sensing, Aussois, France, 18-22 January 1988 (ESA SP-287, April 1988), pp. 87-91.

[2] K. Steffen, "Bidirectional reflectance of snow at 500-600 nm," Large Scale Effects of Seasonal Snow Cover, Proceedings of the Vancouver Symposium, August 1987, IAHS Publ. nr. 166, pp. 415-425.

[3] J.-G. Winther, "Spectral bi-directional reflectance of snow and glacier ice measured in Dronning Maud Land, Antarctica," Annals of Glaciology, Vol. 20, 1994, pp. 1-5.

[4] D.K. Hall, J.L. Foster and A.T.C. Chang, "Reflectance of snow as measured in situ and from space in Sub-Arctic areas in Canada and Alaska," IEEE Transactions on Geoscience and Remote Sensing, Vol. 30, No. 3, May 1992, pp. 634-637.

[5] D.K. Hall, J.L. Foster, J.R. Irons and P.W. Dabney, "Airborne bidirectional radiances of snow-covered surfaces in Montana, USA," Annals of Glaciology, Vol. 17, 1993, pp. 35-40.

[6] T. Guneriussen (ed.), et al., Research and development of remote sensing methods for snow hydrology, Final Report, NORUT IT Report 431/47-00, ISBN 82-7747-107-6, May 2000.